Contents lists available at ScienceDirect

Biochemical and Biophysical Research Communications

journal homepage: www.elsevier.com

Biophysical characterization of histone H3.3 K27M point mutation

Szabolcs Hetey[a], Beáta Boros-Oláh[a], Tímea Kuik-Rózsa[a], Qiuzhen Li[a], Zsolt Karányi[b], Zoltán Szabó[b], Jason Roszik[c], Nikoletta Szalóki[d], György Vámosi[d], Katalin Tóth[e, 1], Lóránt Székvölgyi[a, *, 1]

[a] MTA-DE Momentum, Genome Architecture and Recombination Research Group, Research Centre for Molecular Medicine, Department of Biochemistry and Molecular Biology, University of Debrecen, Debrecen 4032, Hungary
[b] Department of Internal Medicine, University of Debrecen, Debrecen 4032, Hungary
[c] Departments of Melanoma Medical Oncology and Genomic Medicine, The University of Texas MD Anderson Cancer Center, 1515 Holcombe Blvd, Houston, TX 77030, USA
[d] Department of Biophysics and Cell Biology, University of Debrecen, Debrecen 4032, Hungary
[e] DKFZ, Biophysics of Macromolecules, D-69120 Heidelberg, Germany

ARTICLE INFO

Article history:
Received 14 June 2017
Accepted 20 June 2017
Available online xxx

Keywords:
H3.3 K27M
Glioblastoma
Ezh2

ABSTRACT

Lysine 27 to methionine (K27 M) mutation of the histone variant H3.3 drives the formation of an aggressive glioblastoma multiforme tumor in infants. Here we analyzed how the methionine substitution alters the stability of H3.3 nucleosomes *in vitro* and modifies its kinetic properties in live cells. We also determined whether the presence of mutant nucleosomes perturbed the mobility of the PRC2 subunit Ezh2 (enhancer-of-zeste homolog 2). We found that K27 M nucleosomes maintained the wild-type molecular architecture both at the level of bulk histones and single nucleosomes and followed similar diffusion kinetics to wild-type histones in live cells. Nevertheless, we observed a remarkable differential recovery of Ezh2 in response to transcriptional stress that was accompanied by a faster diffusion rate of the mobile fraction of Ezh2 and a significantly increased immobile fraction, suggesting tighter chromatin binding of Ezh2 upon transcription inhibition. The differential recovery of Ezh2 was dependent on transcription, however, it was independent from K27 M mutation status. These biophysical characteristics shed more light on the mechanism of histone H3.3 K27M in glioma genesis in relation to the kinetic properties of Ezh2.

1. Introduction

Lysine 27 to methionine (K27 M) substitution of the *H3F3A* gene, encoding the replication-independent histone variant H3.3, was the first somatic histone gene mutation implicated in tumor development [1–3]. H3.3 K27M nucleosomes drive the formation of the highly aggressive and difficult-to-treat juvenile brain tumor, pediatric glioblastoma multiforme (GBM), which becomes manifested through molecular mechanisms that are only partially understood [1,4,5]. The lysine to methionine substitution was suggested to reduce the catalytic activity of Ezh2, the methyl-transferase subunit of the PRC2 K27 methylase complex, resulting in a global decrease of H3K27 trimethylation and ectopic chromatin binding of Ezh2 [6–8]. Besides catalyzing H3K27 methylation and polycomb-mediated gene repression, Ezh2 also acts as a transcriptional activator by modulating the activity of transcription factors and non-histone substrates [9,10]. *EZH2* mutations have not been observed in pediatric GBM [11]; therefore, it is not clear whether K27 M nucleosomes inactivate Ezh2, mimicking the effect of *EZH2* loss-of-function mutations found in many cancers other than GBM, or perturb the non-canonical (i.e., PRC2-independent) function of Ezh2 associated with transcriptional activation.

In this study, we aimed to determine whether the H3.3 K27M mutation changes the architecture of nucleosomes and interferes with the mobility and transcriptional relationships of histone H3.3 and of Ezh2 within live human cells. We applied various methodologies (single-molecule Förster resonance energy transfer - FRET, fluorescence correlation spectroscopy - FCS, fluorescence recovery after photobleaching - FRAP) to answer these questions.

2. Material and methods

2.1. In vitro nucleosome reconstitution

Mononucleosomes were reconstituted using a salt-dialysis protocol [12]. Widom-601 DNA [13] and recombinant *Xenopus laevis* histones were reconstituted into normal or H3K27 M nucleosomes. The Widom-601 was labeled at −53 nt (Alexa 594) and +41 nt (Alexa 488) with respect to the dyad axis. Octamers were mixed in 2 M NaCl-TE buffer and reconstituted by slow dialysis down to 5 mM NaCl-TE using Slyde-A-Lyzer Mini dialysis tubes (7K MWCO, Thermo-Scientific) and a dialysis bag (Spectrapor 7K).

* Corresponding author.
Email address: lorantsz@med.unideb.hu (L. Székvölgyi)
[1] Senior authors.

http://dx.doi.org/10.1016/j.bbrc.2017.06.133
0006-291/

2.2. Bulk and single-pair FRET experiments

For bulk FRET, a Typhoon 9400 fluorescence scanner (GE Healthcare) was used to determine proximity ratios at the level of nucleosome populations. Samples at different NaCl concentrations were incubated in 384-well microplates prior to measurement and measured in triplicates. The final concentration of labeled nucleosomes was ~1 nM. All images were acquired with 100 μm pixel resolution such that the image plane was set 3 mm above the scanner surface. Fluorescence emission was detected in three spectral channels: donor channel (excitation at 488 nm, detection at 500–540 nm); acceptor channel (excitation at 532 nm, detection at 595–625 nm); energy transfer channel (excitation at 488 nm, detection at 595–625 nm). Detection voltages of the two photomultiplier tubes (PMT) were set between 600 and 700 V. Using the Image Quant software, the proximity ratios were calculated based on intensity values of each acquired image and plotted against the increasing NaCl concentration. Correction factors were determined prior to each measurement. In the spFRET setup, the final concentration of labeled nucleosomes was ~50 pM supplemented with 250 pM of unlabeled nucleosomes. Experiments were carried out using a specific confocal system [14] illuminated continuously with a 491 nm laser (Cobold) for excitation. Prior to burst analysis the nucleosomes were incubated with or without an Ezh2 complex (Active Motif) for 60 min at room temperature. The confocal volume was calibrated with Alexa 488 fluorophore using an ALV5000/E autocorrelator (ALV-Laser GmbH. Langen, Germany), and autocorrelation curves were fitted. After donor excitation fluorescence emission was separated into two detection windows for donor (520–560 nm) and acceptor (>600 nm). Emitted photons were collected by two avalanche photodiodes (APD, Perkin Elmer Optoelectronics). Single molecule bursts were collected by TimeHarp2000 (PicoQuant), and analyzed by the software Frettchen [14,15], where one burst was defined as a group of at least 50 photons with a mutual separation of less than 120 μs? Proximity ratio (P) histograms were plotted based on the selected single events and analyzed by IGOR Pro software (WaveMetrics). P is related to the energy transfer efficiency depending on the distance between the fluorophores.

$$P = N_A / \left(N_A + N_D \right)$$

where N_A and N_D represent the number of detected photons in the respective channels. In both spFRET and bulk systems the correction factors (background and cross talk) needed for P determination were determined in independent measurements.

2.3. Cell culture and transfection

HeLa cells were grown in RPMI-1640 (Sigma, R5886) supplemented with 10% (v/v) fetal calf serum, 2 mM glutamine, penicillin and streptomycin, in 5% CO_2 humidified chamber. H3.3 K27M point-mutation was introduced into a pEGFP-N1-H3.3 and pmCherry-N1-H3.3 plasmid [16], using the quick change mutagenesis technique. *EZH2* was PCR amplified from the NM_004456 (EZH2) Human cDNA ORF Clone (OriGene), and the amplicon was cloned into a pEGFP-N1 and pmCherry-N1 plasmid, respectively. Transient and stable transfections were carried out by Lipofectamine 2000 (Invitrogen) or polyethylenimine PEI-B [17]. Where indicated, cells were pre-treated for 60 min with actinomycin D (5 μg/ml), cycloheximide (20 μg/ml) and flavopiridol (100 nM).

2.4. Confocal laser scanning microscopic (CLSM) analysis

HeLa cells were fixed with 1% formaldehyde prior to each measurement. Images were acquired using an Olympus FluoView 1000 confocal microscope supplied with a 60 × oil immersion objective (NA 1.35). Excitation and emission filters were as follows: EGFP, 488 nm excitation, 500–540 nm detection; mCherry, 543 nm excitation, 600–680 nm detection. Ten optical slices (0.7–1.1 μm) were collected from each nucleus, applying the Kalman filter mode to reduce noise and alternative excitation to exclude crosstalk. Colocalization between Ezh2-mCherry and H3.3-EGFP or H3.3 K27M-EGFP was computed by the JACoP plugin in ImageJ [18].

2.5. Fluorescence recovery after photobleaching

FRAP measurements were performed in HeLa cells using an Olympus FluoView 1000 confocal microscope, based on an inverted IX-81 stand with an UPlanAPO 60 × (NA 1.2) water immersion objective. EGFP was excited by the 488-nm Argon-ion laser line and fluorescence was detected through a 500–550 nm band-pass filter. In the histone FRAP measurements, EGFP-H3.3 or EGFP-H3.3 K27M HeLa cells were randomly selected and five pre-bleach images were taken (256 × 256-pixel area, 10 × zoom, ~9 μW laser power at the objective), which was followed by a 500 ms bleach period of 100% laser power (900 μW). Rectangular areas were selected as bleach ROIs. In the first 90 min, images were acquired every 10 min and then every 30 min, up to 420 min (7 h). Transcription was inhibited by flavopiridol (flav, 100 nM) or actinomycin D (act D, 5 μg/ml), while translation was repressed by cycloheximide (CHX, 20 μg/ml). The drugs were added 60 min before the onset of measurements. Actinomycin D caused a significant (~90%) loss of the initial (pre-bleach) EGFP signal, preventing the long-term tracking of fluorescence recoveries. At these time-points, FRAP recoveries were not calculated. FRAP experiments on Ezh2-EGFP was performed under similar conditions to those on histones, except that fluorescence signal was tracked for 10 s.

2.6. Fluorescence correlation spectroscopy

FCS measurements on histones. HeLa cells were transfected by H3.3-EGFP or H3.3 K27M-EGFP and analyzed by a special fluorescence fluctuation microscope [19]. Fluorescence excitation of EGFP was elicited by a Cobold laser (at 491 nm, 5–15 μW outgoing power, 1 μW excitation power at the objective). EGFP emission was detected through a 515–545 nm band-pass filter using an avalanche photodiode (APD). Measurements were performed at 37 °C.

FCS measurements on Ezh2. An Olympus FluoView 1000 confocal microscope was used and autocorrelation curves were calculated by an ALV-5000E correlation card at three randomly selected points of each nuclei, with 10 × 8 s runs. Measurements were performed at room temperature (22 °C).

FCS data processing and autocorrelation curve fitting. The QuickFit 3.0 software was used (Krieger, Jan; http://www.dkfz.de/Macromol/quickfit/) applying a 3D normal diffusion model for two-component fitting:

$$G(\tau) = \frac{1}{N}\left[\rho_1\left(1+\frac{\tau}{\tau_1}\right)^{-1}\left(1+\frac{\tau}{\gamma^2\tau_1}\right)^{-\frac{1}{2}} + \rho_2\left(1+\frac{\tau}{\tau_2}\right)^{-1}\left(1+\frac{\tau}{\gamma^2\tau_2}\right)^{-\frac{1}{2}}\right]$$

where τ is the lag time, τ_{tr} is the triplet correlation time, τ_1 and τ_2 are the diffusion times of the fast and slow species, ρ_1 and $\rho_2 = 1 - \rho_1$ are the fractional amplitudes of the two components, N is the average number of molecules in the detection volume, and γ is the aspect ratio of the ellipsoidal detection volume. Autocorrelation curves distorted by aggregates floating through the focus were excluded from the analysis.

3. Results

3.1. Characterization of H3 K27 M nucleosomes by FRET

To determine how lysine 27 to methionine substitution affects the stability of H3 K27 M nucleosomes, we introduced the K27 M point mutation into a recombinant histone H3 and expressed all the core histones (H2A, H2B, H3, H3 K27 M, and H4) in *E. coli* (Fig. 1). Purified histone proteins were assembled into wild-type and K27 M octamers, then combined and reconstituted into nucleosomes with a Selex 601 (Widom 601) positioning DNA [17]. Fluorescent tags were incorporated into the Widom 601 sequence creating suitable donor/acceptor fluorophore pairs for subsequent FRET analyses. We measured the equilibrium stability of wild-type and K27 M nucleosomes by microplate-scanning (bulk) FRET [25], allowing us to obtain structural and kinetic information about the assembly of nucleosomes in the time range of minutes. Energy transfer proximity ratios (P) were computed at gradually increasing salt concentrations that elicited nucleosome disassembly in a controlled way (Fig. 1/b). By comparing the dissociation kinetics of wild-type and mutant samples we found a small reduction in the salt-dependent stability of K27 M nucleosomes; however, the difference was not statistically significant. Supplementing the reconstituted nucleosomes with a recombinant Ezh2-complex (Ezh2, EED, Suz12) resulted in no detectable change in nucleosome stability (Fig. S1). Since the properties of individual nucleosomes are averaged in bulk FRET measurements, subtle differences might remain undetected over the whole molecular assembly process. Therefore, we repeated the salt dissociation measurements using single-pair FRET (spFRET), allowing us to track potential sub-populations. In the spFRET setup, 50 pM fluorescent nucleosomes were mixed with 250 pM of unlabeled nucleosomes, and proximity ratio histograms were recorded for a range of salt concentrations (Fig. 1/c and Fig. S2). At the level of individual nucleosomes, the disassembly process did not reveal a significant difference or structural heterogeneity between wild-type and K27 M nucleosomes. We conclude that H3.3 K27M nucleosomes maintain a canonical molecular architecture.

3.2. Functional analysis of H3.3 K27M nucleosomes in live cells

H3.3 K27M mutation has a dominant negative character in humans [6], which makes functional studies possible in the genetic context of endogenous (wild-type) H3.3 expression. We tagged Ezh2 with mCherry and co-expressed the fusion protein with H3.3-EGFP or H3.3 K27M-EGFP (Fig. 2/a). We used confocal laser scanning microscopy (CLSM) to analyze the distribution of Ezh2-mCherry in relation to H3.3-EGFP and H3.3 K27M-EGFP (Fig. 2). Based on the Manders' colocalization coefficients [18,21], about half of the Ezh2 pool overlapped with histone H3.3 or H3.3 K27M, while the other half occupied distinct nuclear compartments (Fig. 2/b and Supplementary Fig. S3). The pattern of colocalization and genomic distribution of Ezh2 was not changed significantly by the K27 M mutation, or upon transcriptional inhibition elicited by actinomycin D and flavopiridol treatments.

Next, we performed kinetic measurements to assess the diffusional properties of Ezh2, H3.3 and H3 K27 M histones at various spatial and temporal resolutions (Figs. 3–4). By FRAP analysis we studied HeLa cells stably expressing histone H3.3-EGFP or H3.3 K27M-EGFP (histone FRAP), and Ezh2-EGFP in the presence of wild-type or K27 M mutant histones (Ezh2 FRAP). The transcription-dependence of H3.3-EGFP/K27 M and Ezh2-EGFP mobility was assessed by comparing control and transcriptionally stressed HeLa cells. The time-range of measurements was two-fold: at the scale of hours (up to 8 h) for the core histone molecules (histone FRAP, Fig. 3/a), and at the scale of seconds (Ezh2 FRAP, Fig. 3/b) for the fast Ezh2 molecules, recovering as fast as most transcription factors [22,23]. In the histone FRAP experiments, nascent protein synthesis was inhibited by cycloheximide (CHX) to avoid the perturbing effect of newly translated histone-EGFP molecules. We found that the recovery of H3.3/K27M-EGFP fluorescence did not reach the initial pre-bleach value such that most histone molecules remained in the slowly exchanging fraction (Fig. 3/a). Actinomycin D increased the immobile (unrecovered) fraction of H3.3 and H3.3 K27M (from 55% to 85%), suggesting strong and direct chromatin binding requiring the process of transcription. Interestingly, the pTEFb (transcriptional elongation factor) inhibitor flavopiridol [24] did not change significantly the repopulation rate of H3.3/K27 M nucleosomes, implying that nascent RNA elongation was dispensable for the chromatin binding of H3.3. The same general pattern was observed after cycloheximide treatment, i.e., most recovery events involved preexisting histones. As opposed to the more static histone molecules, Ezh2-EGFP fully recovered in less than 10 s under normal growth conditions, lacking an apparent immobile fraction (Fig. 3/b). Flavopiridol and actinomycin D treatments induced the formation of a stable immobile fraction of Ezh2 (15% and 35%, respectively). This suggests that Ezh2 has a non-canonical cellular pool that is associated with active transcription, but it is independent from H3.3 K27M mutation.

To scale up the temporal and spatial resolution of our measurements and gain kinetic information in the sub-second time range and sub-micrometer distance range, we applied FCS (Fig. 4) allowing us to track several diffusion parameters. From the rate and frequency of fluorescence intensity fluctuations we computed the time-dependent autocorrelation function (G(τ)), fitted with a 3D normal diffusion model, supposing two autonomous diffusing components (Fig. 4/a and Supplementary Fig. S5). The average ratio of fast components, corresponding to the fraction of molecules freely diffusing across the nucleoplasm, was 61% (SD = 19) for H3.3-EGFP and 56% (SD = 20) for H3.3 K27M-EGFP, respectively (Fig. 4/b, left panel). The proportion of mobile pool increased by 10% after actinomycin D treatment ($p < 0.05$) in the case of H3.3 K27M. The average diffusion coefficient (D) was the same for wild-type and K27 M mutant histones (31 ± 19 μm^2/s and 29 ± 16 μm^2/s) and it was not affected by transcription inhibition (act D) or impaired protein synthesis (CHX) (Fig. 4/b, middle panel). The average fraction of the fast component was ~60% for Ezh2-EGFP (Fig. 4/c, left panel), which slightly increased in the presence of H3.3 K27M-mCherry ($p < 0.05$) and after tran-

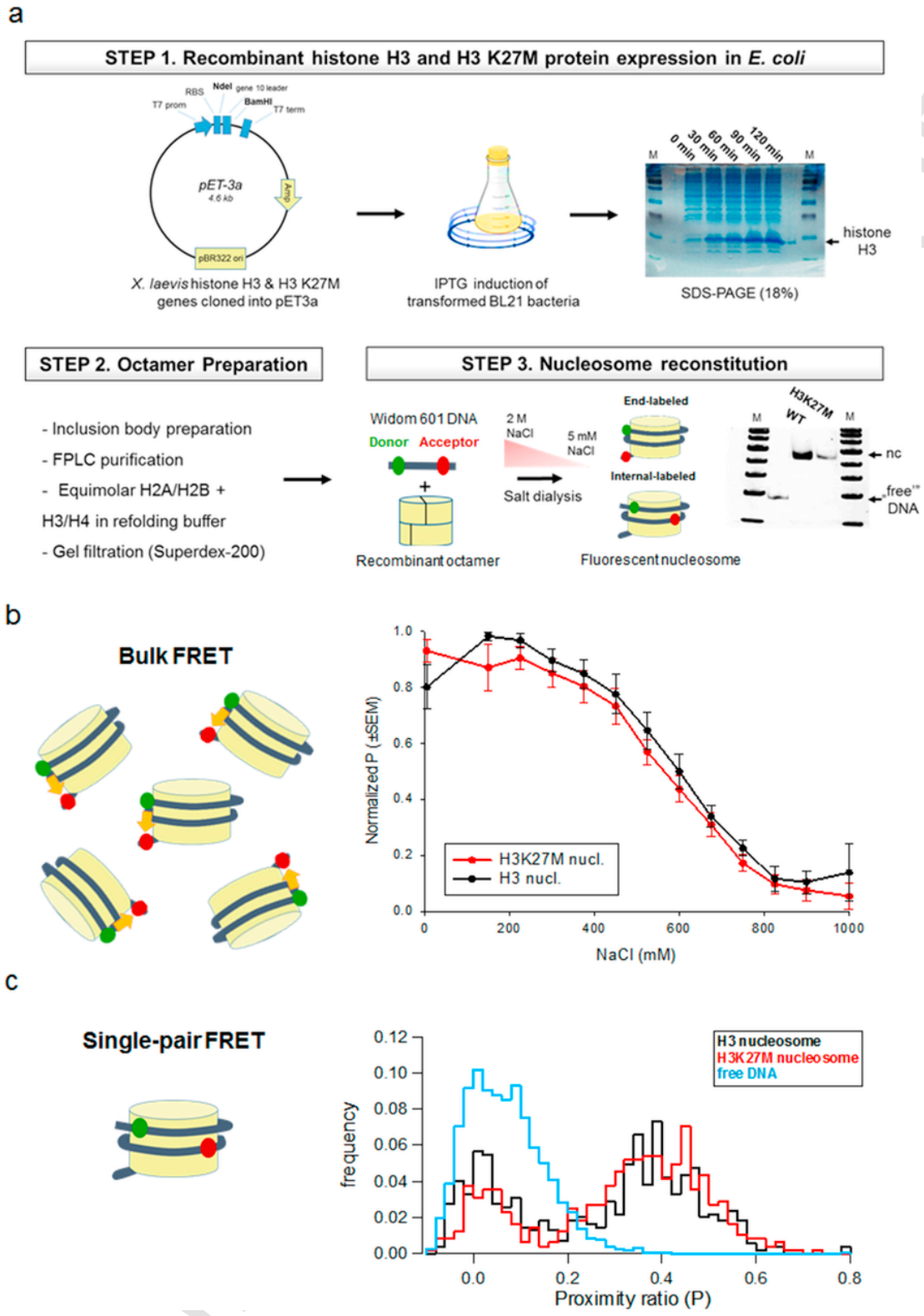

Fig. 1. FRET analysis of reconstituted nucleosomes. (a) Schematic workflow of the experiment. nc: reconstituted nucleosome, M: 100 bp ladder. (b) Salt-dependent destabilization of wild-type (black) and H3K27 M (red) nucleosomes measured by bulk FRET. The decrease of proximity ratios (P) reflects nucleosome dissociation. Dots represent the mean of five independent experiments (±SEM). (c) Distribution of P on single nucleosomes measured by single-pair FRET. Wild-type (black) and H3K27 M (red) nucleosomes, and free DNA (blue) were measured in parallel at various salt concentrations. One representative measurement performed at 5 mM NaCl is shown. Intact nucleosomes appear at a P of ~0.4. (For interpretation of the references to colour in this figure legend, the reader is referred to the web version of this article.)

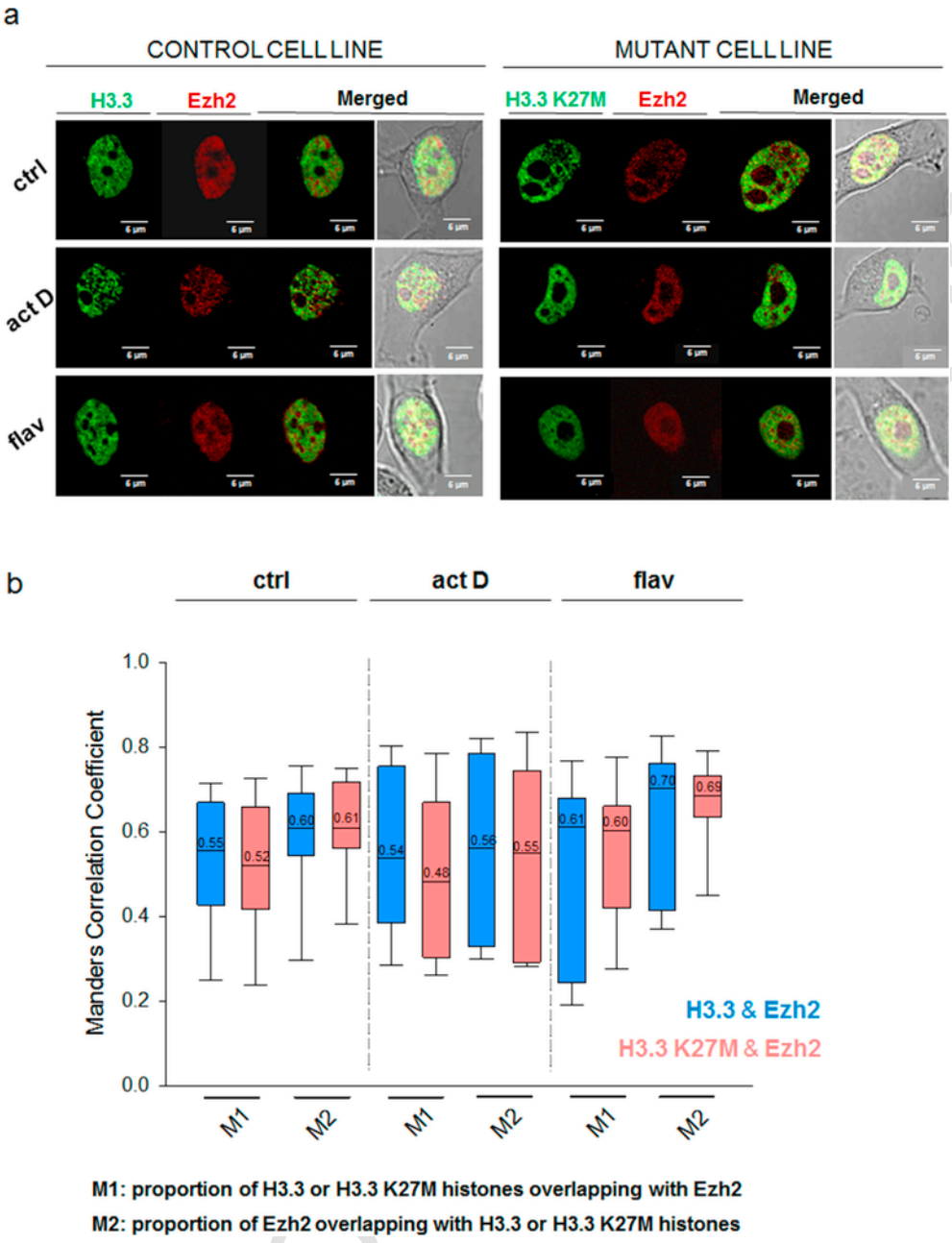

Fig. 2. Microscopic analysis of H3.3 K27M nucleosomes in relation to Ezh2. CLSM was performed in HeLa cells expressing H3.3-EGFP or H3.3 K27M-EGFP (green) and Ezh2-mCherry (red). Representative optical stacks are shown. Scale bar: 5 μm. (a) Nuclear distribution of H3.3-EGFP/H3.3 K27M-EGFP and Ezh2-mCherry under normal growth conditions (ctrl) and after transcriptional inhibition induced by actinomycin D (act D, 5 μg/ml, 60 min) or flavopiridol (flav, 100 nM, 60 min). (b) Quantification of colocalization between H3.3-EGFP/H3.3 K27M-EGFP and Ezh2-mCherry based on the Manders correlation coefficient. For statistical comparison, two-tailed t-tests were performed at a level of significance of 0.05 (*$p < 0.05$). The number of cases (N) was ≥60. (For interpretation of the references to colour in this figure legend, the reader is referred to the web version of this article.)

scription inhibition by flavopiridol ($p < 0.05$). The latter pool of Ezh2-EGFP also had a higher mobility (Fig. 4/c, middle panel), reflected by the increased diffusion coefficients of flavopiridol inhibited cells ($p < 0.05$). This suggests that the nuclear mobility of Ezh2 is significantly restrained by transcription elongation, independently from the presence of H3.3 K27M mutation.

When the diffusion coefficients of the fast populations were converted into apparent molecular masses (based on the Stokes-Einstein equation for spherical objects [25]), there was no significant difference between the real and apparent masses of H3/H3 K27M-EGFP molecules (55.9 kDa/49.26 kDa vs. 42.26 kDa) (Fig. 4/b, right panel), however, Ezh2-EGFP gave ~10-fold larger molecular mass than the real molecular mass of the fusion protein (1.221 kDa/1.900 kDa vs. 102.36 kDa, Fig. 4/c, right panel). This difference reflects that Ezh2 is part of large protein complexes. The apparent molecular masses were not affected by the presence of K27 M mutation.

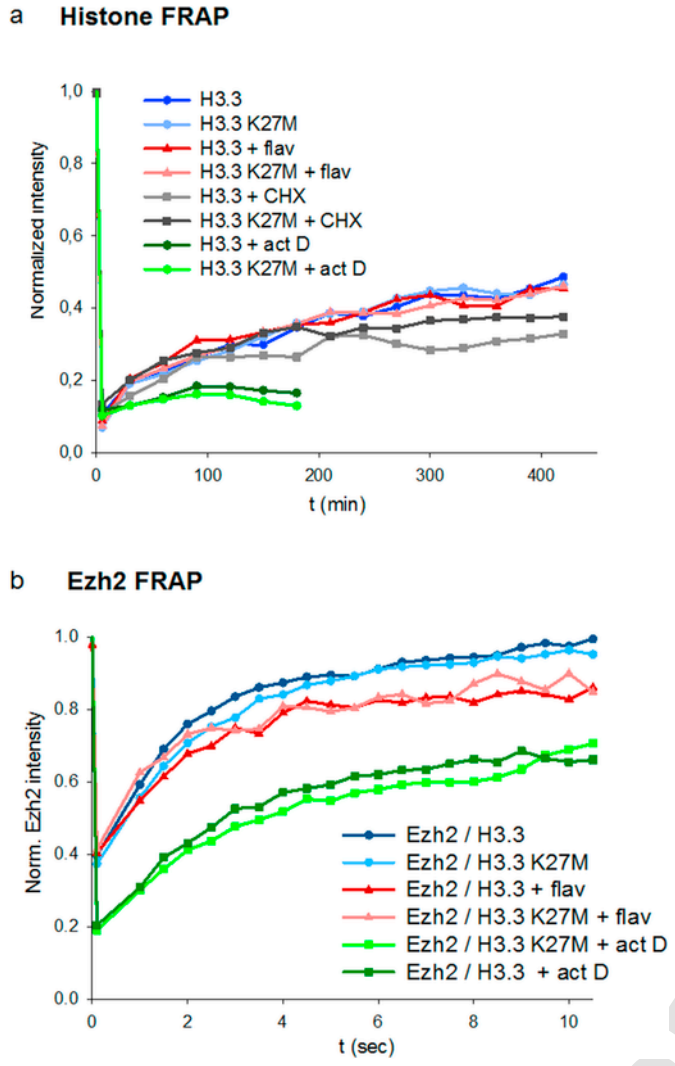

Fig. 3. Measuring the kinetics of H3.3 K27M nucleosomes and Ezh2 in live cells: a FRAP approach. (a) FRAP curves of histone H3.3-EGFP and H3.3 K27M-EGFP, expressed in live cells under normal growth conditions and after transcriptional and translational inhibition. Transcription and translation were inhibited by flavopiridol (flav, 100 nM)/actinomycin D (act D, 5 μg/ml) and cycloheximide (CHX, 20 μg/ml), respectively. The drugs were added 1 h before the measurements. (b) Recovery curves of Ezh2-EGFP in the presence of wild-type (H3.3-mCherry) or mutant (H3.3 K27M-mCherry) nucleosomes.

4. Discussion

Evidence is emerging that epigenetic mutations disrupting post-translational histone modifications play an etiological role in the development of cancer. Earlier studies showed that selective changes of single amino acids or histone tail clipping (in molecular dynamics simulations) significantly altered the stability and dynamic properties of nucleosome core particles [26–28]; however, similar structural rearrangements have not been investigated in the case of H3.3 K27M. Another crucial point is related to Ezh2 that stimulates the expression of a number of target genes independently from its H3K27 methylase activity [11]. The switch between the repressive and stimulatory roles of the double-facet protein Ezh2 is not understood at the molecular level.

Herein we found that K27 M nucleosomes maintained their wild-type molecular architecture and stability, suggesting that single amino acid substitution of the N-terminal H3 tail domain did not cause detectable rearrangements in the structure of NPCs In live human cells, K27 M nucleosomes followed similar diffusion kinetics to their wild-type counterparts and fully recapitulated the slow kinetics and tight chromosome binding of canonical (replication-dependent) H3 molecules [29]. Nevertheless, by FRAP and FCS we found a remarkable differential recovery of Ezh2 in response to transcriptional stress that was accompanied by a significantly increased immobile fraction and faster diffusion rate of the mobile fraction of Ezh2. The differential recovery of Ezh2 was dependent on transcription, however, it was independent from K27 M mutation status. The lack of a significant adverse effects of K27 M is consistent with the recent demonstration of the ability of other post-translational histone modifications surrounding the lysine 27 residue to detoxify the K27 M mutation *in vivo* [30].

Funding

Grants LP2015-9/2015, CRP/HUN13-01, NKFIH-117670, OTKA K103965, GINOP-2.3.2-15-2016-00024/26/30.

Conflict of interest statement

The authors declare no competing interests in relation to the work described. Sz.H. B·B—O. T.K-R. Q.L. N·Sz. Conceived the experiments, L.Sz. and K.T. conducted the experiments, Sz.H. B·B—O. Gy.V. J.R. Z.Sz. Zs.K. K.T. and L.Sz. analyzed the results, L.Sz. wrote the paper. All authors reviewed the manuscript.

Appendix A. Supplementary data

Supplementary data related to this article can be found at http://dx.doi.org/10.1016/j.bbrc.2017.06.133.

Uncited references

[20].

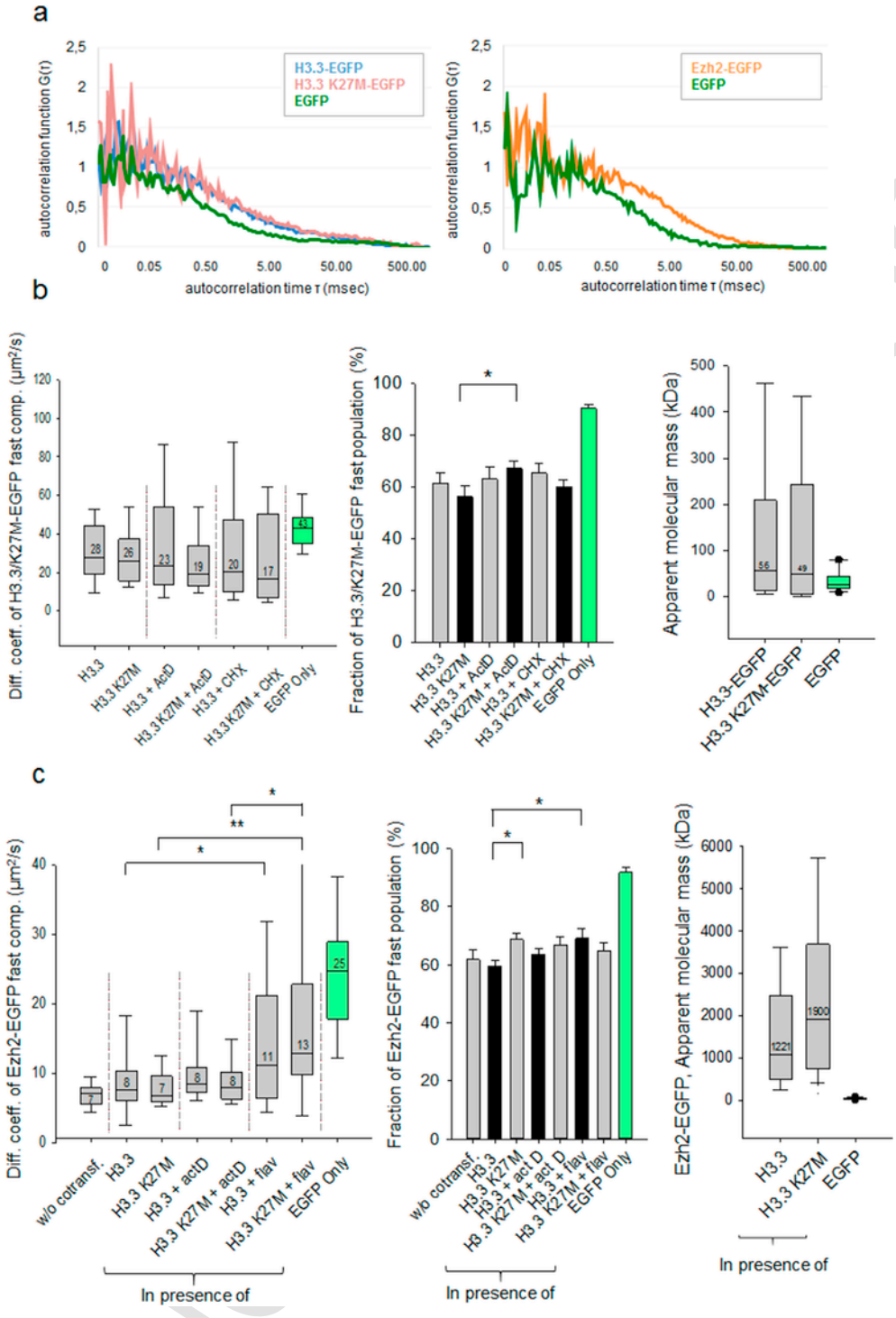

Fig. 4. Measuring the diffusion of H3.3 K27M and Ezh2 by FCS. (a) Representative autocorrelation curves. Histone H3.3-EGFP (blue), histone H3.3 K27M-EGFP (red), Ezh2-EGFP (orange), and EGFP (green). (b) *Left Panel:* Average fraction of the fast diffusion component of H3.3/H3.3 K27M-EGFP under normal metabolic conditions and upon transcription or translation inhibition (actinomycin D (act D, 5 µg/ml), and cycloheximide (CHX, 20 µg/ml)). Significant difference is indicated (*$p < 0.05$, two-tailed *t*-test). The number of cases (N) analyzed was ≥28. Error bar: SEM. Median values are indicated in the boxplots. *Middle Panel:* Distribution of diffusion coefficients of H3.3/H3.3 K27M-EGFP after two-component fitting. *Right Panel:* Distribution of apparent molecular masses of H3.3/H3.3 K27M-EGFP, and EGFP. (c) *Left Panel:* The average fraction of fast diffusion components of Ezh2-EGFP in the presence of wild type (H3.3-mCherry) or mutant (H3.3 K27M-mCherry) histones under normal metabolic conditions and upon transcription inhibition (actinomycin D (act D, 5 µg/ml), and flavopiridol (flav, 100 nM)). Statistical significance is indicated (*$p < 0.05$). *Middle Panel:* Distribution of diffusion coefficients of Ezh2-EGFP in the presence of wild-type (H3.3-mCherry) or mutant (H3.3 K27M-mCherry) histones. Statistical significance is indicated (*$p < 0.05$; **$p < 0.001$, Mann-Whitney rank sum test). *Right Panel:* Distribution of apparent molecular masses of Ezh2-EGFP in the presence of wild-type (H3.3-mCherry) or mutant (H3.3 K27M-mCherry) histones, or EGFP. (For interpretation of the references to colour in this figure legend, the reader is referred to the web version of this article.)

References

[1] D. Sturm, et al., Hotspot mutations in H3F3A and IDH1 define distinct epigenetic and biological subgroups of glioblastoma, Cancer Cell. 22 (2012) 425–437.

[2] J. Schwartzentruber, et al., Driver mutations in histone H3.3 and chromatin remodelling genes in paediatric glioblastoma, Nature 482 (2012) 226–231.

[3] S. Bender, Y. Tang, A.M. Lindroth, V. Hovestadt, D.T.W. Jones, M. Kool, M. Zapatka, P.A. Northcott, D. Sturm, W. Wang, B. Radlwimmer, J.W. Højfeldt, D. Castel, S. Schubert, M. Ryzhova, S. Huriye, Reduced H3K27me3 and DNA hypomethylation are major drivers of gene expression in K27M mutant pediatric high-grade gliomas, Cancer Cell. 24 (2013) 660–672.

[4] G. Wu, A. Broniscer, T. a McEachron, C. Lu, B.S. Paugh, J. Becksfort, C. Qu, L. Ding, R. Huether, M. Parker, J. Zhang, A. Gajjar, M. a Dyer, C.G. Mullighan, R.J. Gilbertson, E.R. Mardis, R.K. Wilson, J.R. Downing, D.W. Ellison, J. Zhang, S.J. Baker, Somatic histone H3 alterations in pediatric diffuse intrinsic pontine gliomas and non-brainstem glioblastomas, Nat. Genet. 44 (2012) 251–253.

[5] D.-A. Khuong-Quang, P. Buczkowicz, P. Rakopoulos, X.-Y. Liu, A.M. Fontebasso, E. Bouffet, U. Bartels, S. Albrecht, J. Schwartzentruber, L. Letourneau, M. Bourgey, G. Bourque, A. Montpetit, G. Bourret, P. Lepage, A. Fleming, P. Lichter, M. Kool, A. von Deimling, D. Sturm, A. Korshunov, D. Faury, D.T. Jones, J. Majewski, S.M. Pfister, N. Jabado, C. Hawkins, K27M mutation in histone H3.3 defines clinically and biologically distinct subgroups of pediatric diffuse intrinsic pontine gliomas, Acta Neuropathol. 124 (2012) 439–447.

[6] P.W. Lewis, M.M. Müller, M.S. Koletsky, F. Cordero, S. Lin, L. a Banaszynski, B. a Garcia, T.W. Muir, O.J. Becher, C.D. Allis, Inhibition of PRC2 activity by a gain-of-function H3 mutation found in pediatric glioblastoma, Science 340 (2013) 857–861.

[7] K. Chan, D. Fang, H. Gan, R. Hashizume, C. Yu, M. Schroeder, N. Gupta, S. Mueller, C.D. James, R. Jenkins, J. Sarkaria, Z. Zhang, The histone H3. 3K27M mutation in pediatric glioma reprograms H3K27 methylation and gene expression, Genes Dev. 27 (2013) 1–6.

[8] N. Justin, Y. Zhang, C. Tarricone, S.R. Martin, S. Chen, E. Underwood, V. De Marco, L.F. Haire, P.A. Walker, D. Reinberg, J.R. Wilson, S.J. Gamblin, Structural basis of oncogenic histone H3K27M inhibition of human polycomb repressive complex 2, Nat. Comm. 7 (2016) 11316.

[9] D.B. Yap, J. Chu, T. Berg, M. Schapira, S.-W.G. Cheng, A. Moradian, R.D. Morin, A.J. Mungall, B. Meissner, M. Boyle, V.E. Marquez, M.A. Marra, R.D. Gascoyne, R.K. Humphries, C.H. Arrowsmith, G.B. Morin, S.A.J.R. Aparicio, Somatic mutations at EZH2 Y641 act dominantly through a mechanism of selectively altered PRC2 catalytic activity, to increase H3K27 trimethylation, Blood 117 (2011) 2451–2459.

[10] S. Varambally, S.M. Dhanasekaran, M. Zhou, T.R. Barrette, C. Kumar-Sinha, M.G. Sanda, D. Ghosh, K.J. Pienta, R.G.A.B. Sewalt, A.P. Otte, M.A. Rubin, A.M. Chinnaiyan, The polycomb group protein EZH2 is involved in progression of prostate cancer, Nature 419 (2002) 624–629.

[11] R.R. Lulla, A.M. Saratsis, R. Hashizume, Mutations in chromatin machinery and pediatric high-grade glioma, Sci. Advences 2 (2016) e1501354.

[12] K. Luger, T.J. Rechsteiner, T.J. Richmond, Preparation of nucleosome core particle from recombinant histones, Methods Enzymol. 304 (1999) 3–19.

[13] P. Lowary, J. Widom, New DNA sequence rules for high affinity binding to histone octamer and sequence-directed nucleosome positioning, J. Mol. Biol. 276 (1998) 19–42.

[14] A. Gansen, K. To, N. Schwarz, Structural variability of nucleosomes detected by single-pair förster resonance energy transfer: histone acetylation, Sequence Var. Salt Eff. (2009) 2604–2613.

[15] A. Gansen, K. Tóth, N. Schwarz, J. Langowski, Opposing roles of H3- and H4-acetylation in the regulation of nucleosome structure—a FRET study, Nucleic Acids Res. 43 (2015) 1433–1443.

[16] E. Delbarre, B.M. Jacobsen, A.H. Reiner, A.L. Sørensen, P. Collas, Chromatin environment of histone variant H3. 3 revealed by quantitative imaging and genome-scale chromatin and DNA immunoprecipitation, Mol. Biol. Cell. 21 (2010) 1872–1884.

[17] P.A. Longo, J.M. Kavran, M.-S. Kim, D.J. Leahy, Transient mammalian cell transfection with polyethylenimine (PEI), (n.d.).

[18] S. Bolte, F.P. Cordelieres, A guided tour into subcellular colocalisation analysis in light microscopy, J. Microsc. 224 (2006). 13–232.

[19] N. Dross, C. Spriet, M. Zwerger, G. Mü Ller, W. Waldeck, J. Rg Langowski, J.Z. Rappoport, Mapping eGFP oligomer mobility in living cell nuclei, PLoS One 4 (2009).

[20] A. Gansen, A.R. Hieb, V. Bohm, K. Toth, J. Langowski, Closing the gap between single molecule and bulk FRET analysis of nucleosomes, PLoS One 8 (2013).

[21] K.W. Dunn, M.M. Kamocka, J.H. McDonald, A practical guide to evaluating colocalization in biological microscopy, Am. J. Physiol. Cell Physiol. 300 (2011) C723–C742.

[22] M. Dundr, U. Hoffmann-Rohrer, Q. Hu, I. Grummt, L.I. Rothblum, R.D. Phair, T. Misteli, A kinetic framework for a mammalian RNA polymerase in vivo, Science 298 (2002) 1623–1626 (80-.).

[23] R.D. Phair, S.A. Gorski, T. Misteli, Measurement of dynamic protein binding to chromatin in vivo, using photobleaching microscopy, Methods Enzymol. 375 (2004) 393–414.

[24] M.V. Blagosklonny, Flavopiridol, an inhibitor of transcription: implications, problems and solutions, Cell Cycle 3 (2004) 1537–1542.

[25] P. Brazda, T. Szekeres, B. Bravics, K. Toth, G. Vamosi, L. Nagy, Live-cell fluorescence correlation spectroscopy dissects the role of coregulator exchange and chromatin binding in retinoic acid receptor mobility, J. Cell Sci. 124 (2011) 3631–3642.

[26] A. Flaus, C. Rencurel, H. Ferreira, N. Wiechens, T. Owen-Hughes, Sin mutations alter inherent nucleosome mobility, EMBO J. 23 (2004) 343–353.

[27] H. Neumann, S.M. Hancock, R. Buning, A. Routh, L. Chapman, J. Somers, T. Owen-Hughes, J. van Noort, D. Rhodes, J.W. Chin, A method for genetically installing site-specific acetylation in recombinant histones defines the effects of H3 K56 acetylation, Mol. Cell. 36 (2009) 153–163.

[28] M. Biswas, K. Voltz, J.C. Smith, J. Langowski, Role of histone tails in structural stability of the nucleosome, PLoS Comput. Biol. 7 (2011) 1–12.

[29] H. Kimura, P.R. Cook, Kinetics of core histones in living human Cells : little exchange of H3 and H4 and some rapid exchange of H2B, 153 (2001) 1341–1353.

[30] Z.Z. Brown, M.M. Müller, S.U. Jain, C.D. Allis, P.W. Lewis, T.W. Muir, Strategy for "Detoxification" of a cancer-derived histone mutant based on mapping its interaction with the methyltransferase PRC2, J. Am. Chem. Soc. 136 (2014) 13498–13501.